Article

Broadband Dielectric Spectroscopic Detection of Aliphatic Alcohol Vapors with Surface-Mounted HKUST-1 MOFs as Sensing Media [†]

Papa K. Amoah [1,2], Zeinab Mohammed Hassan [3], Rhonda R. Franklin [4], Helmut Baumgart [1,2], Engelbert Redel [5] and Yaw S. Obeng [6,*]

[1] Department of Electrical and Computer Engineering, Old Dominion University, Norfolk, VA 23529, USA
[2] Applied Research Center at Thomas Jefferson National Accelerator Laboratories, 12050 Jefferson Avenue, Suite 721, Newport News, VA 23606, USA
[3] Chemistry Department, Faculty of Science, Fayoum University, P.O. Box 63514, Fayoum 63514, Egypt
[4] Department of Electrical and Computer Engineering, University of Minnesota, 200 Union Street SE, Minneapolis, MN 55455, USA
[5] Institute of Functional Interfaces (IFG), Karlsruhe Institute of Technology, Hermann-von-Helmholtz-Platz 1, 76344 Eggenstein-Leopoldshafen, Germany
[6] Physical Measurement Laboratory, National Institute of Standards and Technology, 100 Bureau Drive, Gaithersburg, MD 20899, USA
* Correspondence: yaw.obeng@nist.gov
[†] Contribution of the National Institute of Standards and Technology, not subject to copyright.

Abstract: We leveraged chemical-induced changes to microwave signal propagation characteristics (i.e., S-parameters) to characterize the detection of aliphatic alcohol (methanol, ethanol, and 2-propanol) vapors using TCNQ-doped HKUST-1 metal-organic-framework films as the sensing material, at temperatures under 100 °C. We show that the sensitivity of aliphatic alcohol detection depends on the oxidation potential of the analyte, and the impedance of the detection setup depends on the analyte-loading of the sensing medium. The microwaves-based detection technique can also afford new mechanistic insights into VOC detection, with surface-anchored metal-organic frameworks (SURMOFs), which is inaccessible with the traditional coulometric (i.e., resistance-based) measurements.

Keywords: broadband dielectric microwave spectroscopy; TCNQ-HKUST-1 SURMOF, thin film sensing material; HKUST-1 metal–organic framework (MOF) sensing material; aliphatic alcohol vapor detection; VOC detection

1. Introduction

Chemical sensors are based on reversible and proportional changes in physicochemical properties of the detector when exposed to the target analyte [1,2]. In addition, most gas sensors must be cost effective and usable in rather harsh conditions [3]. Emerging gas sensors based on metal-organic frameworks (MOFs) appear to meet these criteria [4]. These MOFs could potentially address the difficulties with selectivity [5] that

limit other sensor materials [6]; in principle, the charge transfer processes in these MOF materials which result in altering band structures are similar to those in the metal-oxide semiconductor, and could be suitable as gas sensors [2,6]. In addition, MOFs are highly porous materials which are able to form coordination complex clathrate-like structures with gas molecules, making them ideal for selective gas sensors [7–10]. HKUST-1 surface-coordinated MOF thin films (SURMOF) doped with TCNQ is a well characterized platform for investigating selective gas detection [7,11,12]. Indeed, it has been shown elsewhere [13] that the thermal conductivities of SURMOF are commensurate with their

single crystalline MOF analogues, and decrease in the presence of adsorbates, due to increased vibrational scattering and guest molecule-induced hybridization of low frequency modes [14]. When coupled with emerging transient electrical techniques, these MOF platforms enable highly selective and ultra-trace gas-phase sensing. For example, AC-impedance spectroscopy has been used in combination with optimized hydrophobic MOF to selectively detect iodine with part-per-billion (ppb) level sensitivity [15]; the microwave resonant cavity technique has been used to detect and distinguish between methanol, ethanol, and acetone in the 0–200 ppm range at room temperature [16]; and HKUST-1-like Cu-BTC nanoparticles have been used in the capacitive sensing of VOCs [7]. We have also demonstrated elsewhere that in contrast to the traditional coulometric techniques, surface mounted ZnO nanotubes, and HKUST SURMOF, can sense ethanol at temperatures under 100 °C, using broadband microwave dielectric spectroscopy (BDS) [17,18]. While gas monitoring with such emerging metrology has been demonstrated, the performance metrics such as selectivity, sensitivity, reproducibility, and long-term stability are not yet well established. Furthermore, the impact of such environmental factors as temperature and humidity are currently not well understood [19]. Thus, there is a need to improve our fundamental knowledge of these metrology tools such as microwave gas sensors.

In this study, we investigated broadband dielectric spectroscopy (BDS) [20], in combination with TCNQ-doped HKUST-1 SURMOF, to sense aliphatic alcohol and acetone vapors. In the following, we first investigate the alcohol vapor analyte access (i.e., size limited loading) to the reactive metal sites in the SURMOF for detection. We then compare the thermodynamic- and kinetic-controlled analyte uptake by the SURMOF sensing medium from the responses of neat solvents and 1:1 v/v methanol - ethanol mixture. Finally, we investigate the proposed cooperative electrocatalytic oxidation mechanism by comparing the responses of the aliphatic alcohols and acetone. We expect acetone to react differently from alcohols as the former cannot form the prerequisite alkoxide intermediate, under the experimental conditions [21].

1.1. Broadband Dielectric Spectroscopy (BDS) Background

Broadband dielectric spectroscopy (BDS) [20] rapidly interrogates a wide range of material physicochemical characteristics through the movement of dipoles in the presence of an external electric field such as microwaves (MW). It measures the material under test's (MUT's) complex relative permittivity (i.e., dispersive and dissipative dielectric behavior) in response to the rapidly changing electrical and magnetic fields, which in simple one-component systems is mainly due to dielectric polarization [22]. Thus, BDS should lend itself well to the electronic detection of volatile organic compounds (VOCs) as they invariably involve changes in polarizability, including, but not limited to, changes in bond polarizability [18]. The microwave signal is scattered by the analyte (i.e., MUT) according to the material's permittivity. The signal reflecting from the electrical connections and transmitted between the two connectors is summarized as a matrix of scattering parameters (S-parameters). These parameters capture how RF energy travels through a multiport network, such as using a vector network analyzer (VNA), with the analyte between the source and receiver. Thus, the output of the S-parameters is convoluted with the transfer function of the sensor loaded with the MUT, i.e., (h(f)) [23]; thus, the S-parameters can be deconvoluted to produce the circuit elements characteristic of the analyte [24].

In this work, we used the S-parameters to evaluate the chemo-induced changes (CIC) that result from the volatile organic compounds (VOCs, e.g., aliphatic alcohols) adsorbed on the SURMOF sensing materials, by measuring the MW insertion loss characteristics of the transmitted signal (S_{21}) as a function of the experimental variables. In the experimental configuration used, the sensing material was interrogated by the interaction of the electric fields which are emitted from the signal line, located in the center of the electrode, and terminated on the two ground lines adjacent to the signal line of the coplanar waveguide (GSG CPW). The electric fields reaching the sensing materials can be approximated as a planar field. With this approximation, the microwave insertion loss (i.e., S_{21}) measures the

fraction of energy that is transmitted from the source (port 1) to the detector (port 2) through the device under test (DUT) with the gas sensing device on top. In our experimental setup, the device under test (DUT, comprised of the waveguide, end-launchers, and the MUT) matched very well to the characteristic impedance (Z_0) of the VNA; it had very low reflections (S_{11}/S_{22}) [25]. Thus, with proper calibration, the S_{21} amplitude and phase can be correlated to the total impedance of the GSG CPW waveguide and gas sensing device.

2. Experimental

2.1. Preparation of the TCNQ Doped HKUST-1 MOF Sensing Material Preparation

Polycrystalline SURMOF was grown in a layer-by-layer (LbL) fashion on plasma-activated borosilicate SiO_2 glass substrates as described elsewhere [14,26]. Before MOF deposition, the glass substrates were cleaned with ethanol and activated with O_2 plasma cleaning. The MOF precursors, i.e., the copper acetate solution (1.0 mM) and the benzene-1,3,5-tricarbixylic acid (BTC) linker (0.2 mM), were subsequently sprayed on the substrate with spraying times of 15, and 25 s, respectively, followed by a rinsing step with pure EtOH for 5 s for each spray deposition cycle. By varying the number of spray cycles, the HKUST-1 film thickness could be easily tuned; in this work the thickness of SURMOF was ≈35 nm, formed from 30 spray cycles [27].

The 7,7,8,8-tetracyano-quinodimethane (TCNQ) loading of fresh HKUST-1 SURMOF was accomplished as described in the open literature [28,29]. The greenish color of our films is indicative of mixed valent Cu^{2+}/Cu^+ defects [30] that form reactive adducts with dioxygen molecules, and are probably responsible for the catalytic aerobic oxidative properties of the HKUST-1 SURMOF [31]. The samples were diced into 1.5 cm by 2.5 cm pieces and stored in a pure nitrogen atmosphere prior to use.
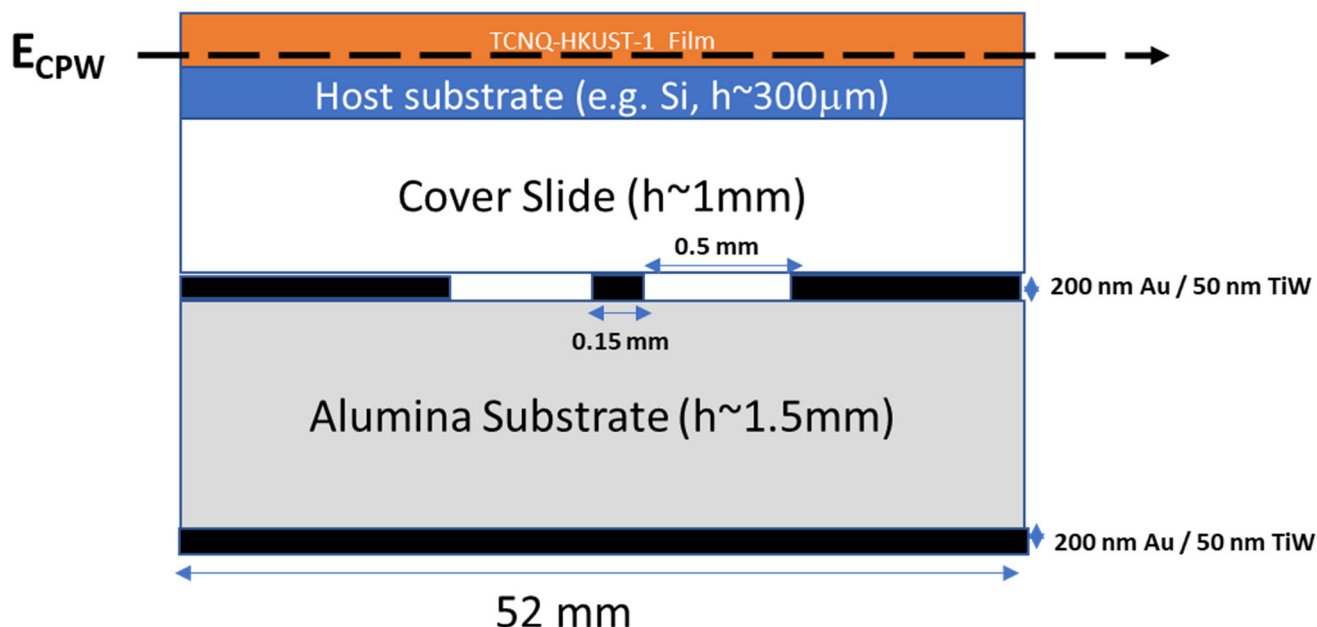
Analytical grade solvents—methanol, ethanol, 2-propanol, and acetone—were obtained from Sigma-Aldrich (Milwaukee, St. Louis, MO, USA), and were used as received.

2.2. BDS Setup and Measurements

In this work, we used a ground–signal–ground (GSG) coplanar waveguide (CPW) fabricated from gold-covered alumina (1 mm thick polished alumina (dk 9.5)). The cables from the CPW to the vector network analyzer (VNA, SPARQ 4004E, Teledyne LeCroy, Chestnut Ridge, NY, USA) were connected through edge mount connectors (Model 1492-04A-6, Southwest Microwave, Tempe, AZ, USA). This configuration effectively converts the coaxial mode signal of the cable into a coplanar waveguide mode propagating towards the material under test (MUT). A two-port short-open-load-through (SOLT) calibration is used to shift the VNA reference plane to end of the connector/cable interface by attaching the calibration standards to the ends of the cables. The cables connecting to the CPW were de-embedded, moving the reference plane of the measurement from the port faces of the VNA to the connector/cable interface. Thus, the device under test (DUT) is defined as two launch connectors and the CPW itself with the MUT on top, and the reported S-parameter data variations are those from experimental perturbations to the MUT. If the SURMOF is deposited on a conductive substrate (e.g., silicon substrate) the sensing substrate is isolated from the gold signal traces by a Corning #1 glass coverslip (Product number CLS284518, Aldrich-Sigma, Milwaukee, WI, USA), as shown in Figure 1 below; otherwise, the glass cover slide is optional.

In this experimental configuration, the sensing material is interrogated by the interaction of the electric fields emanating from the signal line and terminating on the ground lines of the coplanar waveguide. The electric fields reaching the sensing material layer can be approximated as planar given the size of the gap compared to the signal line width in the CPW and distance from the given thicknesses of the silicon substrate and glass coverslip, as shown in Figure 1. With this approximation and proper calibration, the microwave insertion loss (i.e., S_{21}) measures the fraction of energy that is transmitted from the

source to the detector through the MUT, and the S_{21} amplitude can be correlated to the total impedance of the GSG waveguide, the optional glass coverslip, and the SURMOF/Si device [17].
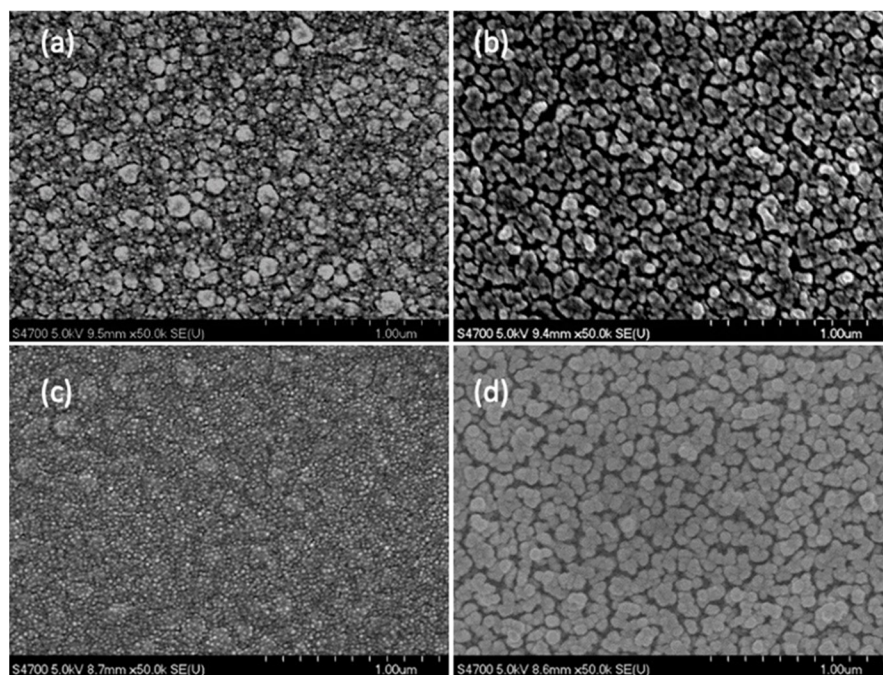

Figure 1. A phenomenological model of a doped HKUST-1 SURMOF under microwave interrogation in a gaseous ambient. E_{CPW} is an electric field fringe from the microwave emanating from the signal line and terminating on the ground line of the GSG CPW. Note that the figure is for illustration only, and not to scale. Some features important features have been deliberately exaggerated for illustrative purposes.

The sample CPW assembly was situated in a resistively heated Pyrex tube reactor, with porous endcaps, that allowed independent control of the environment around the sensing material. The temperature of the assembly can be manually controlled with a power supply from room temperature to approximately 120 °C. For this study, the temperature was maintained at 65 °C to extend the life of the edge mount connectors to the CPW. Both the S-parameters, in the 0.1 to 20 GHz range, and the reactor temperature, were measured every 30 seconds. The response of the BDS system to analyte concentration was investigated by flash vaporizing varying amounts (0.01 to 1.0 mL) of neat analytical grade analyte (i.e., methanol, ethanol, 2-propanol, acetone, and 1:1 volume-by-volume methanol–ethanol mixture) into the reactor using a long-needled hypodermic Hamilton syringe [18]. Saturation (over 1000 ppm) was observed in the test chamber for solvent amounts of 0.01 ml of solvent in the temperature window used in this study. The system response was monitored for five minutes after each dosing followed by a five-minute ambient gas purge before the next aliquot of solvent was injected. Although a broad range of frequencies was monitored, selected reporting frequencies were chosen based on the experimental setup, the sample dimensions, and the molecular species of interest[14]. We quantified energy dissipation into the sensing material by calculating the microwave attenuation constant (α) (i.e., defined as the real part of the microwave propagation constant ($\Upsilon = \alpha + j\beta$)), by numerical RLCG modeling [32] using custom MATLAB (MathWorks, Natick, MA, USA) code. Statistical data analysis to determine the impact of the guest molecule loading and gaseous environment on the measurand was performed with JMP software (JMP, SAS Institute, Cary, NC, USA).

Figure 2 compares the plan-view FE-SEM micrographs of HKUST-1 SURMOF thin films grown on borosilicate glass substrates. The main difference between pristine

HKUST-1 SURMOF films and the TCNQ-infiltrated MOF films is that the pristine undoped case exhibits large crystalline domains interspersed by many much smaller grains, while the TCNQ-doped SURMOFs films show a uniformly distributed grain size comprised of primarily large grains separated by wide cracks between the MOF domains, which were presumably formed as a result of significant unit-cell changes during the doping [26]. The full characterization of these films is described elsewhere [33]. The pre-existing TCNQ does not prevent the further uptake of other guest molecules by HKUST-1 crystals [34]; hence, we expect the uptake of N_2 or other small Lewis base molecules to be unimpeded by the TCNQ dopant already in the MOF [18,35].
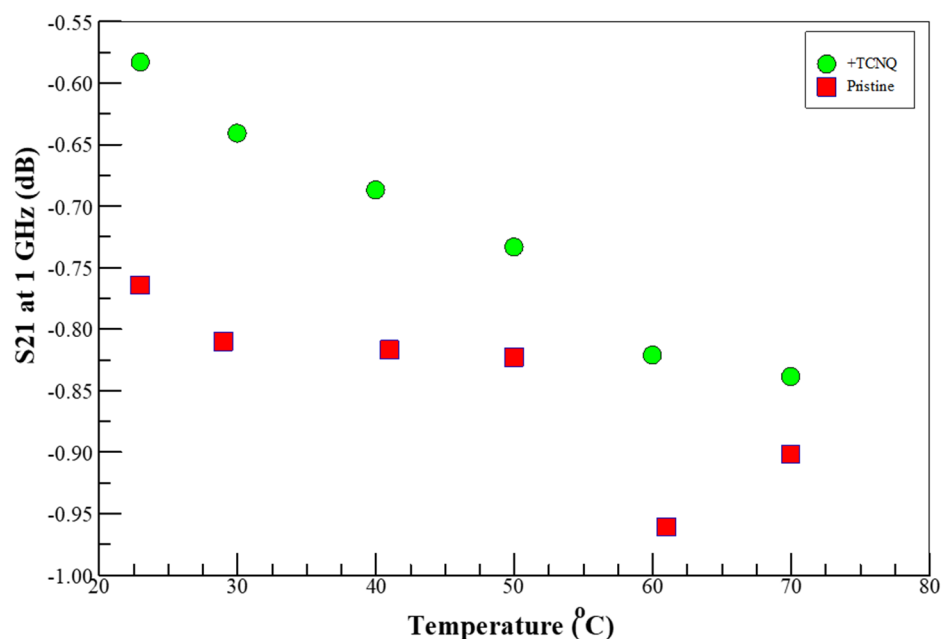

Figure 2. Planar view FE-SEM micrographs of HKUST-1 SURMOF thin films grown on borosilicate glass substrates displaying the differences in MOF morphology between undoped pristine MOFs versus TCNQ-doped MOFs of very loosely stacked MOF grains with very noticeable gaps between individual MOF grains, which are especially pronounced following TCNQ loading of thicker 40 deposition cycles of MOF films: (**a**) 10 cycles pristine MOF; (**b**) 10 cycles TCNQ; (**c**) 40 cycles MOF pristine; and (**d**) 40 cycles MOF with TCNQ-loaded MOF (adapted from [33]).

3. Results and Discussion

3.1. Characterization of the HKUST-1 SURMOF Sensing Material

The electrical conductivity of the doped materials is higher than that of the undoped films due to dopant-induced electronic structural change [36]; Seebeck coefficient measurements show holes as the majority charge carriers in the doped films at room temperature [26,37]. Figure 3 compares the temperature dependence of microwave insertion loss (S_{21} amplitude) for pristine- and TCNQ-doped HKUST-1 SURMOF films on Si, at 1 GHz in a N_2-rich air environments. The doped MOF system becomes more lossy when electron-rich N_2 molecules (Lewis base) coordinate to the open Cu^{2+} centers [35], and reduce the concentration of the majority hole carriers [37]. Furthermore, the temperature sensitivity of the electrical conduction of the doped KHUST-1 material is consistent with guest-induced electronic and vibrational structures changes in the SURMOF [14,38] Specifically, the temperature dependence of the S_{21} in the doped material suggests that either nitrogen adsorption at the open metal sites is limited by heat-induced conformational changes in the MOF cage to allow access to the open metal sites [39,40], or the device has temperature-dependent drifts below 50 °C [41]. By comparison, the poor temperature dependence of the S_{21} of the "pristine" material is more consistent with the electron hopping between

localized orbitals of adjacent metal centers [42,43]. All subsequent experiments were conducted using the TCNQ-doped SURMOF films at 65 °C to avoid the S_{21} drift [18], and to preserve the performance of the end-launchers of the GSG CPW waveguide.
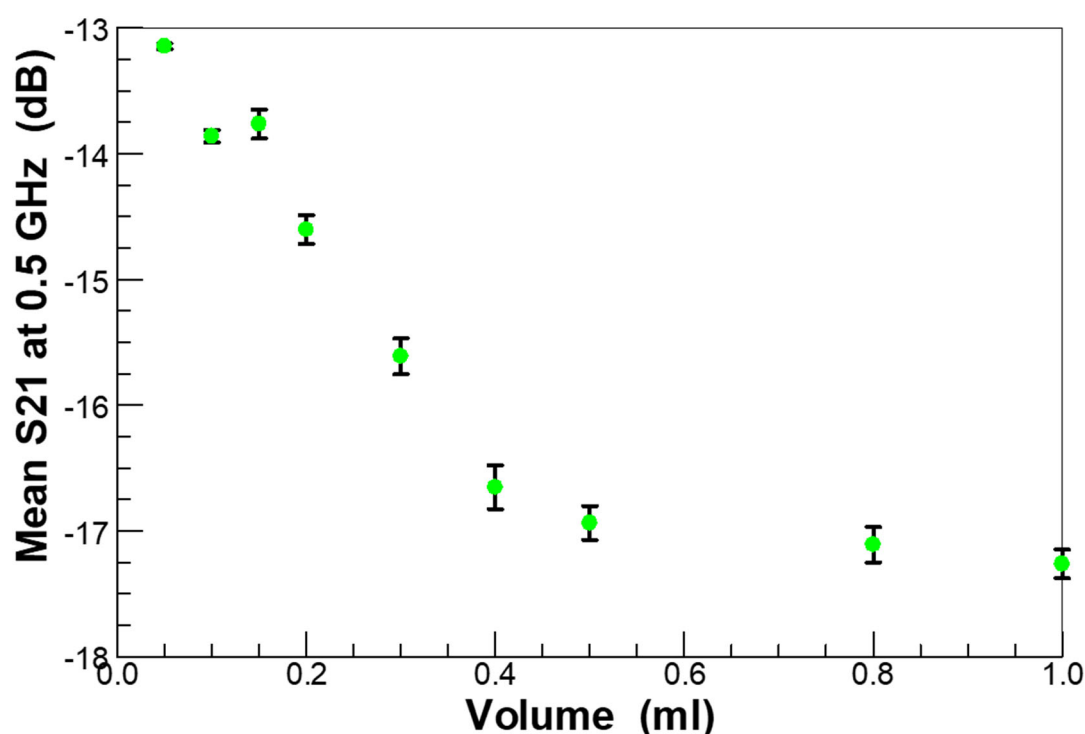

Figure 3. Temperature dependence of microwave insertion loss amplitude (S_{21}) of pristine and TCNQ-doped HKUST-1 SURMOF on Si in a N_2-rich air environments, at 1 GHz. The error bars represent the standard deviation of at least three measurements on the same sample and are substantially smaller than the symbol sizes.

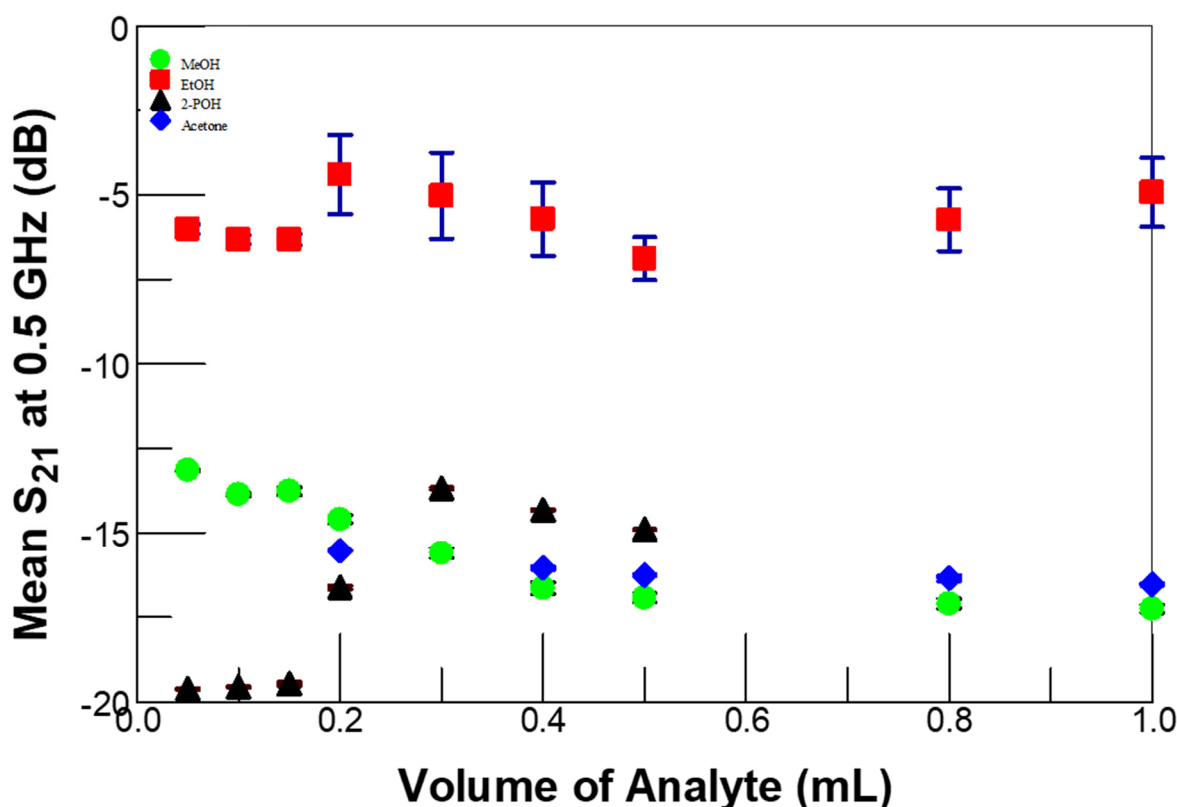### 3.2. Aliphatic Alcohol Oxidation in TCNQ-loaded HKUST-1 MOF

Figure 4 shows the time-averaged and methanol vapor concentration dependence of the insertion loss ($|S_{21}|$) of the TCNQ-doped HKUST-1 MOF in an air ambient at 65 °C. The $|S_{21}|$ depended only on the methanol vapor concentration, as summarized in Figure 5, which is the time-averaged $|S_{21}|$ monitored at 0.5 GHz of methanol vapor concentration dependence on TCNQ-loaded HKUST-1 at 65 °C, in air. The DUT becomes more resistive with increasing volume of solvent flash vaporized into the reactor, and then levels off at around 0.4 ml of neat methanol injected. As in the nitrogen environment, the system becomes more lossy as the electron-rich aliphatic alcohol (Lewis base) associates and donates electrons to the open Cu^{2+} centers [35], and color centers, which results in the reduced concentration of the majority hole carriers.

Figure 4. Methanol concentration dependence of the time-averaged microwave insertion loss amplitude (S_{21}) TCNQ-loaded HKUST-1 SURMOF on Si substrate at 65 °C, purged with pure air, monitored at 0.5 GHz. The error bars represent the standard deviation of at least three five-minute measurements for each aliquot of methanol.
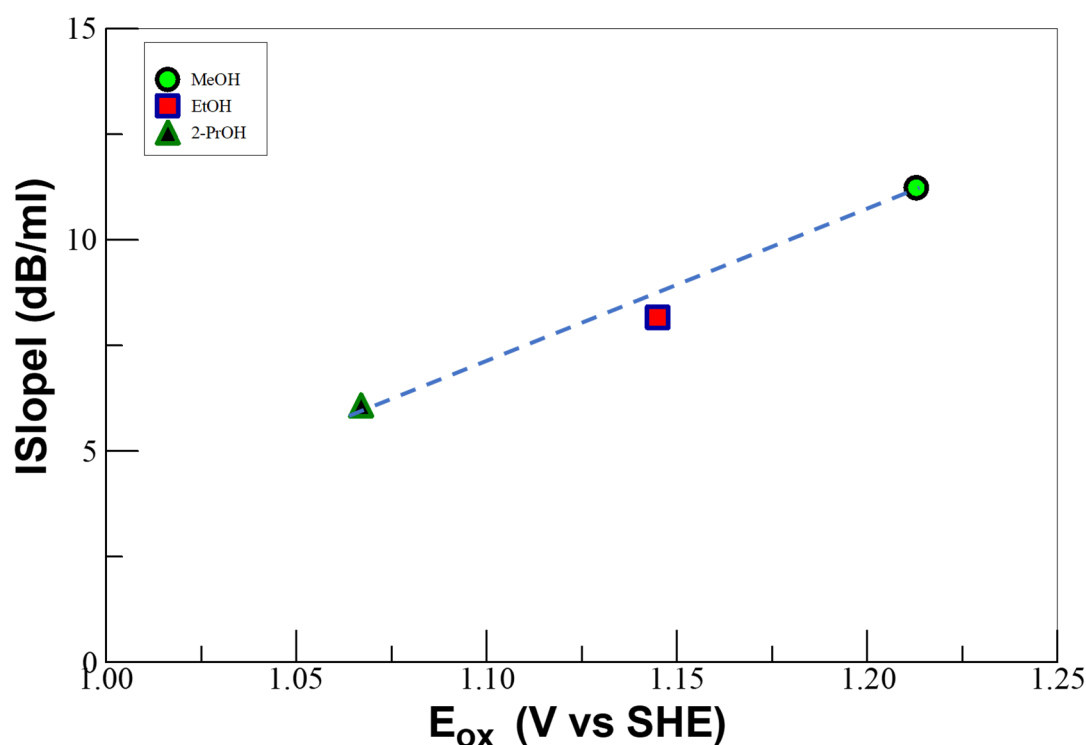
Figure 5 compares the time-averaged insertion loss amplitude (S_{21}) monitored at 0.5 GHz for methanol (MeOH), ethanol (EtOH), 2- propanol (2-PrOH), and acetone as a function of the volume of solvent flash vaporized into the reactor with TCNQ-doped HKUST-1 SURMOF at 65 °C and purged with pure air. Although acetone is not an aliphatic alcohol, it is an oxidation product of 2-propanol and was studied to understand the impact of adsorption/desorption kinetics of the oxidation products in the proposed BDS detection mechanism. The S_{21} amplitude response spanned a wide range, but close inspection shows that all the traces share the salient features of Figure 4: three segments comprised of a subcritical concentration range in which the impedance is quite high, a linear region in which the S_{21} amplitude response is proportional to the analyte concentration, and a saturation segment above which the insertion loss does not appear to depend on the analyte concentration. Table 1 summarizes these features, and some pertinent physico-chemical properties for the solvents studied.

Figure 5. Comparison of analyte concentration dependence of microwave insertion loss amplitude (S_{21}) TCNQ-loaded HKUST-1 SURMOF on Si substrate at 65 °C in air, monitored at 0.5 GHz. The error bars represent the standard deviation of at least three measurements.

In the linear range, the insertion loss amplitude increased (i.e., S_{21}) with increasing analyte concentration, consistent with impedance increases due to the reduction om the majority carrier concentration in the TCNQ-doped HKUST-1 SURMOF [26,37], and is reminiscent of the output of coulometric gas sensors [44]. Furthermore, the linear segment can be fitted to a linear equation (with $R_2 > 0.98$, Prob > t of at least 0.02) with a characteristic slope as summarized in Table 1. As discussed below, the solvent molecules enter the unoccupied subunits within the MOF cage to adsorb at the open Cu^{2+} sites and are subsequently oxidized in a charge transfer (e.g., electrons transferred from the analyte to the metal center). The net electron transfer reaction reduces the hole concentration to alter the conductivity and impedance of the sensor device. While we do not expect the analyte molecules to displace TCNQ from the host, the changes in the impedance suggest some adsorbate-induced changes in the SURMOF. We take the analyte concentration dependence of the $|S_{21}|$ (i.e., the slopes of the linear sections of the traces in Figure 5) as a measure of the ease of oxidation of the adsorbed analyte molecules (i.e., electron donation into the doped MOF complex). Figure 6 shows a correlation between the proposed ease of oxidation, i.e., the slopes of the linear sections of the traces in Figure 5 and representative electrooxidation potentials of the solvents molecules on an arbitral platinum-based catalyst obtained from the literature [45]. The strong correlation suggests that the insertion loss change depends on the thermodynamics of oxidation of the aliphatic alcohol analytes.
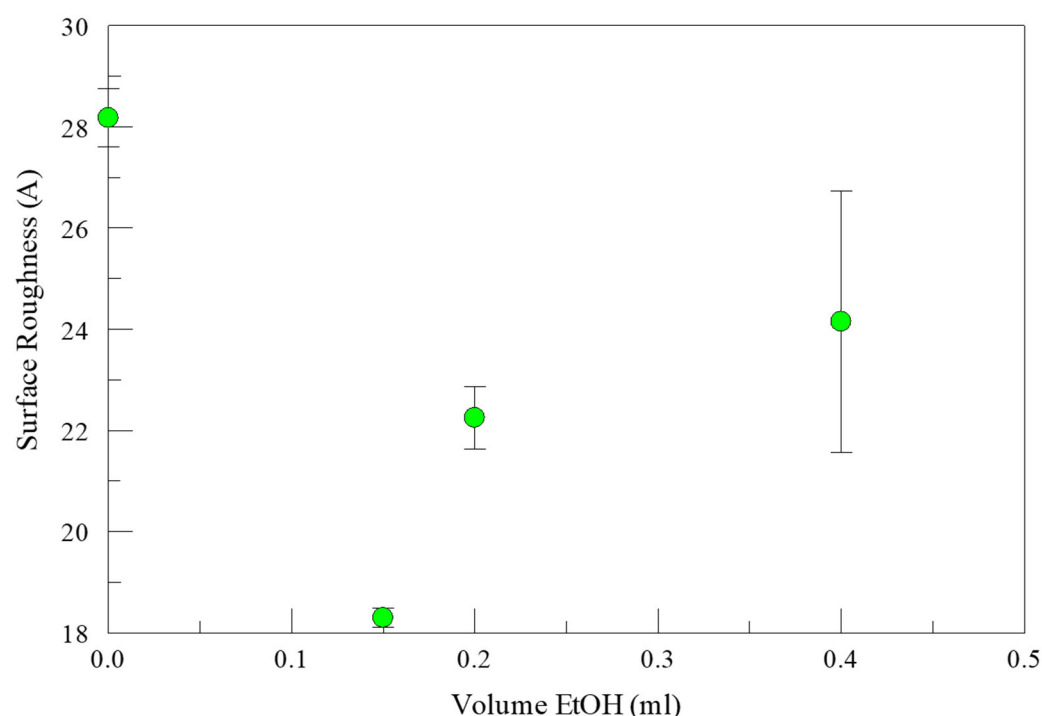
Figure 6. The dependence of the slope of the analyte volume dependence of insertion loss on the electrocatalytic oxidation potential of aliphatic alcohol analytes on a platinum-based catalyst, taken from Lammy et al. [45]. The blue dashed line is just a visual aid.

Table 1. Summary of $|S_{21}|$-concentration plot features, and some salient physico-chemical properties of neat analytes.

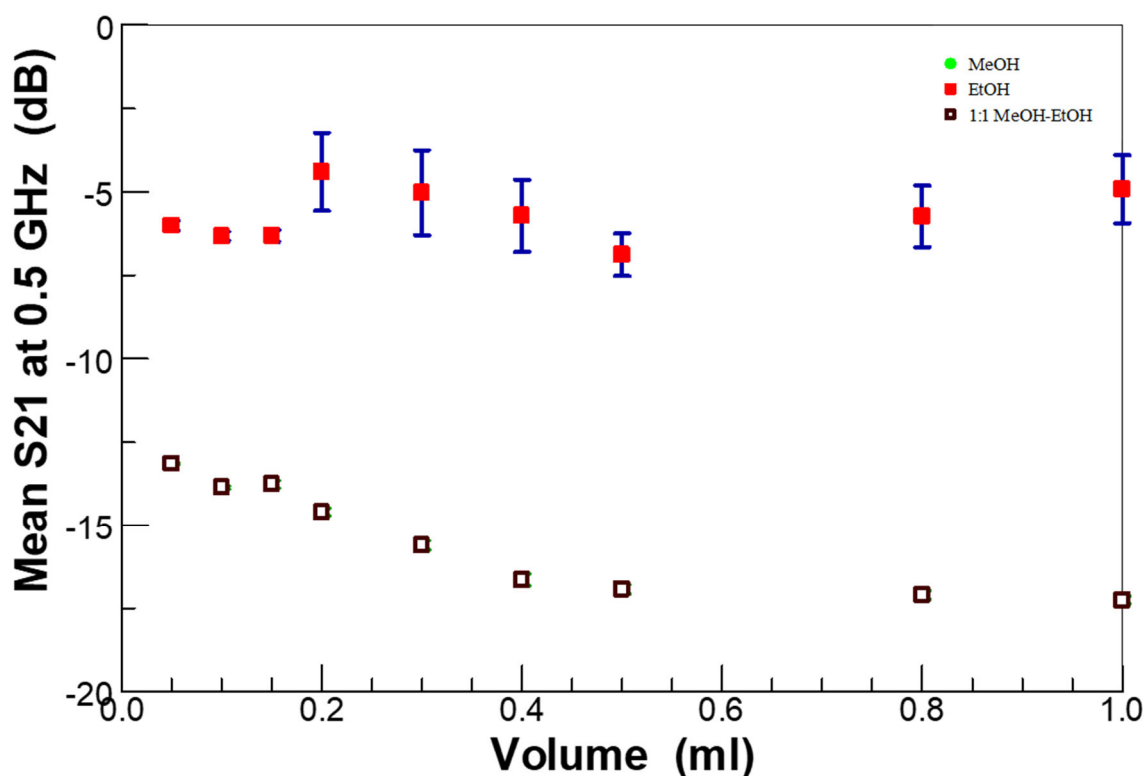| Solvent	Dielectric Constant	Dipole Moment	Acceptor Number	Oxidation Potential (V/SHE) [45]	ΔG (kJmol^{-1})	Lower Detection Limit (ml)	Upper Linear Limit (ml)	Slope (dB/ml)
Methanol	32.7	1.7	41.5	0.016	−9.3	0.1	0.5	−11.228
Ethanol	24.5	1.69	37.9	0.084	−97.3	0.2	0.5	−8.160
2-Propanol	18	1.66	33.5	0.097	−168	0.3	0.5	−6.083
Acetone	20.7	2.85	12.5	−0.879		0.2	0.5	−2.440

In Figure 5, the S_{21} response to injected analyte volumes below 0.2 ml suggest anomalously high impedances, which seem to recover after exposing the films to higher volumes of solvent. Moreover, the $|S_{21}|$-analyte concentration plots for 2-porpoanol, acetone, and methanol exhibit higher impedances than that of ethanol. These observations suggest that other factors, beyond redox thermodynamics, such as reduced mass transport, influence the VOC detection. Solvents are known to plasticize the outer layer of the MOF material, due to MOF destructuring at the film–air interface [12,46,47]. Thus, the reduced mass transport could be due to blocked pores at the film–air interface surface due to solvent-induced modifications of the outer surface of HKUST-1 SURMOF, which impede the uptake and release of solvent by the films. Interestingly, the deconstructed surface can be regenerated when exposed to the synthesis solvents, i.e., ethanol in the case of HKUST-1 SURMOF, to allow improved analyte uptake by the film [12], as shown in Figure 5. Figure 7 shows the atomic force microscope (AFM)-measured surface roughness of HKUST-1 SURMOF films exposed to varying amounts of ethanol vapor at 65 °C. The data show that the initial surface plasticizes when exposed to small volumes of ethanol but recovers with

increasing volumes of solvent exposure. The regeneration of the outer film surface in ethanol explains the observed lower impedances when ethanol is used as the analyte.
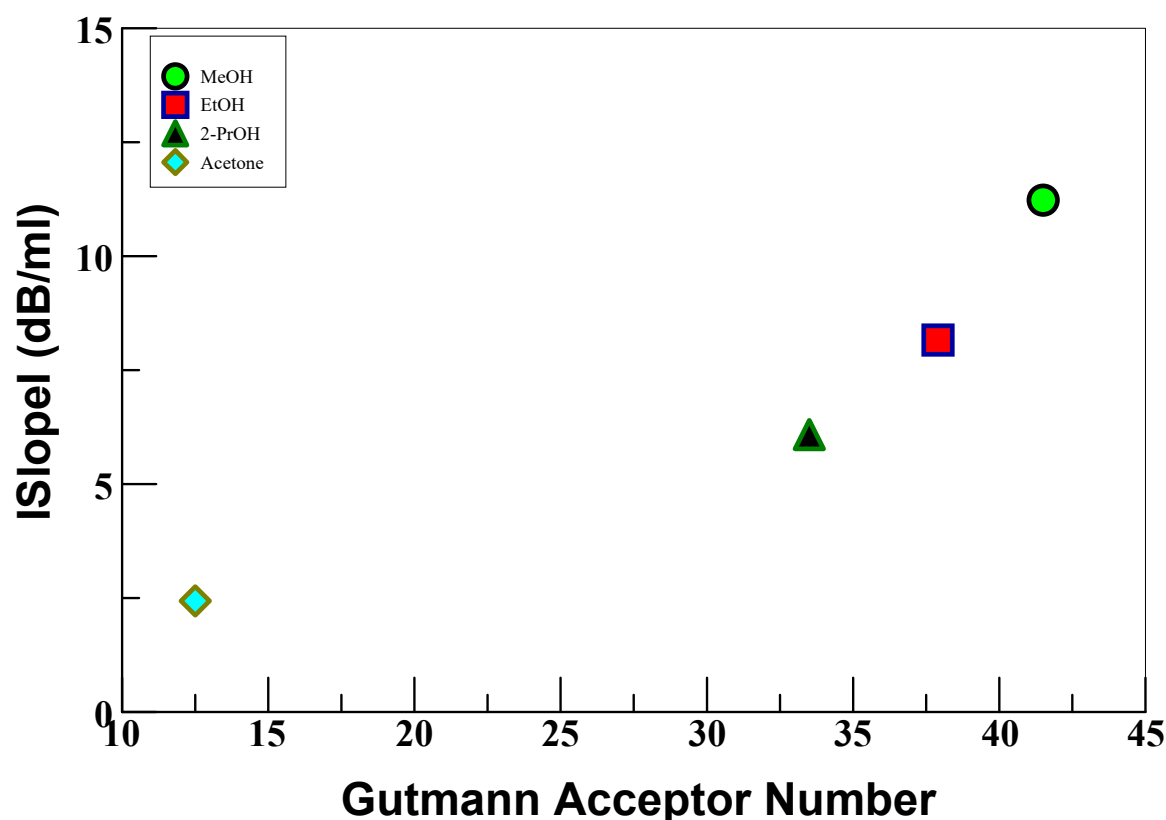

Figure 7. Surface roughness of HKUST-1 SURMOF films exposed to varying amounts of ethanol vapor at 65 °C showing initial surface plasticization and recovery with increasing volumes of solvent. The error bars represent the standard deviation of roughness measurements from at least three distinct areas on the sample surface.

The thermodynamic versus kinetic selectivity of the analyte oxidation was evaluated by challenging a fresh TCNQ-doped HKUST-1 SURMOF sample with a 1:1 volume mixture of methanol and ethanol at 65 °C in air. As shown in Figure 8, the data for the 1:1 MeOH-EtOH mixture, monitored at 0.5 GHz, completely overlap that for neat methanol (MeOH), i.e., the mixture response is identical to that of pure methanol. This indicates that the sensing agent is selective to methanol over ethanol, despite the surface deconstruction, which limits the mass transport of methanol into the pores of the SURMOF. The data also suggest that the methanol selectivity is kinetically driven, probably due to the differences in the analyte diffusion rates to the metal sites; in turn, this is probably due to the SURMOF surface plasticization, as shown in Figure 7.

Figure 8. Comparison of solvent concentration dependence of microwave insertion loss amplitude (S_{21}) TCNQ-loaded HKUST-1 on Si substrate at 65 °C, in air, for methanol (MeOH), ethanol (EtOH), and 1:1 mixture of ethanol and methanol, monitored at 0.5 GHz. The 1:1 MeOH-EtOH symbols completely overlap those for pure methanol (MeOH). The error bars represent the standard deviation of at least three measurements.

Figure 9 shows the relationship between the slope of the analyte volume dependence of insertion loss, i.e., the slopes of the linear sections of the traces in Figure 5, and the Gutmann Acceptor (AN) of the analyte molecules studied, where the AN is a measure of the strength of solvents as Lewis acids [48]. While the alcohol analytes show a linear dependence on the AN, acetone is off the line. This strongly suggests that the alcohol analyte and/or the oxidation products hydrogen bond within the HKUST-1 structure [6], possibly due to the pre-existing dopants at the color centers within the film [30]. This hydrogen bonding may also explain the reduced diffusion of analyte molecules into the MOF film [49]. Taken together, the sensitivity of VOC detection depends on the diffusion rate of the analyte molecule and the ease of charge transfer at the active metal sites.

Figure 9. The relationship between the slope of the analyte volume dependence of insertion loss and the Gutmann Acceptor (AN). AN is a measure of hydrogen bond acidity, and the linear relationship suggests that the analyte molecules and/or the oxidation products form hydrogen bonds within the HKUST-1 structure.

3.3. Proposed Mechanism for BDS Detection of Aliphatic Alcohols in HKUST-1 MOF

Metal organic frameworks have been shown to be efficient electrode modifiers in the selective electro-oxidation of alcohols into carbonyl compounds [50,51] and acids [52]. Analyte ingress and subsequent confinement, within the MOF, appear to be critical to the success of these oxidation reactions. We have previously proposed the following set of conceivable elementary steps involved in the BDS detection of aliphatic alcohols with TCNQ-doped HKUST-1 SURMOF [18].

1. Analyte molecules diffuse into accessible cavities to interact with the open Cu^{2+} active sites, some of which exist as Cu^{2+}-Cu^+-O_2 defects, in the SURMOF. These defects appear to be responsible for many of the electronic properties of the SURMOF films [11,30]. The introduction of the analyte molecules also induces distortion of the mechanical structure, as well as changes in the electronic band structure that lead to changes in the conductivity of the MOF. In a pure nitrogen ambient, the N_2 adsorbs on the metal sites [53], but in the presence of Lewis base molecules, such as aliphatic alcohols, the analyte is expected to displace pre-adsorbed N_2 molecules to form adducts from the open metal sites.

2. The aliphatic alcohol probably associates with the binuclear copper-oxo defects [30], or coordinates to the open metal center, via the hydroxyl-oxygen atom. The confined alcohol analyte is aerobically oxidized by the Cu sites [54] into carbonyl compounds (e.g., aldehydes from the primary) at room temperature [55], with electrons transferred into the MOF from the alcohol. This step is dependent on the presence of oxygen in the ambient conditions within the reactor, which is required for the reoxidation of the Cu(I) to Cu(II). The oxidative abilities HKUST-1 MOF are attributable to the presence of mixed-valent-Cu-oxo defects [31], which behave like aerobic functions

such as in respiration [56]. These mixed valent Cu-oxo centers in the defective MOF are critical for the spontaneous oxidation of alcohols in aerobic conditions [4,57,58].

Mechanistic studies [14,59] of Cu-catalyzed oxidation of alcohols under aerobic conditions suggest an initial hydrogen atom abstraction via a cupric-superoxide complex in which an O-coordinated alcoholate undergoes an H-abstraction reaction from the α-carbon atom of the alcoholate. This generates a bound ketyl radical which then converts intramolecularly into aldehyde, via a one-electron reduction of the Cu (II) into a Cu-I center [60]. Such redox reactions at the metal centers should be readily detected by BDS because of the expected changes in the conductivity of the device under test (DUT) [4]. The resultant carbonyl compounds are also more polarizable and will contribute to the observed increased insertion loss.

The open metal sites in the HKUST-1 MOF, formed by removing axial ligands and or the defective metal sites, strongly coordinate to electron rich species (i.e., Lewis bases). Small molecules, such as short-chained aliphatic alcohols, reversibly adsorb at the available open metal centers in the MOF cavity inducing changes in its physicochemical properties [4,57,61]. The adsorption and reaction at the metal sites also result in changes in interfacial polarization and permittivity, which should be readily detected by microwave energy dissipation [62]. Furthermore, microwave (MW) irradiation is known to promote the rapid and selective oxidation of alcohols to carbonyl compounds as the microwave irradiation promotes faster and more efficient internal heating through direct interaction between microwave energy and the reactants [63–65]. Thus, we expect the adsorbed aliphatic alcohol analyte at the open Cu sites in the host MOF sites to be aerobically oxidized into aldehydes [66] as the basis of VOC detection with MOF thin films [18]. Furthermore, microwave (MW) irradiation is known to rapidly convert alcohols to carbonyl compounds over transition metal catalysts [67], probably due to more efficient internal heating within the reactants [63–65], the creation of localized plasmon resonance-like "hot spots" in the metal support [68], or some specific microwave effects on chemical reactions [69].

4. Conclusions

By observing microwave signal attenuation in different sensor material systems, we demonstrated physics consistent with chemo-induced changes in the electrical properties of the TCNQ-doped HKUST-1 SURMOF sensing media in the detection of volatile solvents (i.e., methanol, ethanol, 2-propanol, and acetone) at 65 °C. The microwave signal attenuation, possibly due to resistance increases, is attributed to majority carrier (hole) annihilation from the electrons donated into the extended hybrid molecular orbital network of the TCNQ-HKUST-1 complex during the analyte oxidation. The VOC analyte specific detection sensitivity depends on the ease of oxidation, i.e., the oxidation potential, of the analyte. Unfortunately, the analyte degrades the surface of the SURMOF to form a plasticized skin that impedes the analyte's diffusion into the porous medium. This results in the underutilization of a tremendous volume of the sensing media.

Technology, nor does it imply that the materials or equipment identified are necessarily the best available for the purpose.

Informed Consent Statement: Not applicable.

Data Availability Statement: The datasets generated during the current study are available from the corresponding author on reasonable request.

Conflicts of Interest: The authors declare no conflict of interest.

References

1. Korotcenkov, G. *Chemical Sensors: Comprehensive Sensor Technologies Volume 4: Solid State Devices*; Momentum Press: New York, NY, USA, 2011.
2. Gopel, W. Chemisorption and charge-transfer at ionic semiconductor surfaces—Implications in designing gas sensors. *Prog. Surf. Sci.* **1985**, *20*, 9–103. https://doi.org/10.1016/0079-6816(85)90004-8.
3. Dey, A. Semiconductor metal oxide gas sensors: A review. *Mater. Sci. Eng. B* **2018**, *229*, 206–217.
4. Zhong, H.; Ghorbani-Asl, M.; Ly, K.H.; Zhang, J.; Ge, J.; Wang, M.; Liao, Z.; Makarov, D.; Zschech, E.; Brunner, E.; et al. Synergistic electroreduction of carbon dioxide to carbon monoxide on bimetallic layered conjugated metal-organic frameworks. *Nat. Commun.* **2020**, *11*, 1409. https://doi.org/10.1038/s41467-020-15141-y.
5. Ma, D.; Li, Z.; Zhu, J.; Zhou, Y.; Chen, L.; Mai, X.; Liufu, M.; Wu, Y.; Li, Y. Inverse and highly selective separation of CO2/C2H2 on a thulium–organic framework. *J. Mater. Chem. A* **2020**, *8*, 11933–11937.
6. Kreno, L.E.; Leong, K.; Farha, O.K.; Allendorf, M.; Van Duyne, R.P.; Hupp, J.T. Metal–organic framework materials as chemical sensors. *Chem. Rev.* **2012**, *112*, 1105–1125. https://doi.org/10.1021/cr200324t.
7. Homayoonnia, S.; Zeinali, S. Design and fabrication of capacitive nanosensor based on MOF nanoparticles as sensing layer for VOCs detection. *Sens. Actuators B Chem.* **2016**, *237*, 776–786.
8. Ali, A.; Alzamly, A.; Greish, Y.E.; Bakiro, M.; Nguyen, H.L.; Mahmoud, S.T. A highly sensitive and flexible metal-organic framework polymer-based H2S gas sensor. *ACS Omega* **2021**, *6*, 17690–17697. https://doi.org/10.1021/acsomega.1c02295.
9. Chowdhury, S.; Torad, N.L.; Ashok, A.; Gumilar, G.; Chaikittisilp, W.; Xin, R.; Cheng, P.; Ul Hoque, M.I.; Wahab, M.A.; Karim, M.R.; et al. Template- and etching-free fabrication of two-dimensional hollow bimetallic metal-organic framework hexagonal nanoplates for ammonia sensing. *Chem. Eng. J.* **2022**, *450*, 138065.
10. Qin, P.; Day, B.A.; Okur, S.; Li, C.; Chandresh, A.; Wilmer, C.E.; Heinke, L. VOC mixture sensing with a MOF film sensor array: Detection and discrimination of Xylene Isomers and their Ternary Blends. *ACS Sensors* **2022**, *7*, 1666–1675. https://doi.org/10.1021/acssensors.2c00301.
11. Heinke, L.; Wöll, C. Surface-mounted metal–organic frameworks: Crystalline and porous molecular assemblies for fundamental insights and advanced applications. *Adv. Mater.* **2019**, *31*, 1806324.
12. Müller, K.; Vankova, N.; Schöttner, L.; Heine, T.; Heinke, L. Dissolving uptake-hindering surface defects in metal–organic frameworks. *Chem. Sci.* **2019**, *10*, 153–160. https://doi.org/10.1039/C8SC03735C.
13. Babaei, H.; DeCoster, M.E.; Jeong, M.; Hassan, Z.M.; Islamoglu, T.; Baumgart, H.; McGaughey, A.J.H.; Redel, E.; Farha, O.K.; Hopkins, P.E.; et al. Observation of reduced thermal conductivity in a metal-organic framework due to the presence of adsorbates. *Nat. Commun.* **2020**, *11*, 4010. https://doi.org/10.1038/s41467-020-17822-0.
14. DeCoster, M.E.; Babaei, H.; Jung, S.S.; Hassan, Z.M.; Gaskins, J.T.; Giri, A.; Tiernan, E.M.; Tomko, J.A.; Baumgart, H.; Norris, P.M.; et al. Hybridization from guest–host interactions reduces the thermal conductivity of metal–organic frameworks. *J. Am. Chem. Soc.* **2022**, *144*, 3603–3613. https://doi.org/10.1021/jacs.1c12545.
15. Babal, A.S.; Mollick, S.; Kamal, W.; Elston, S.; Castrejón-Pita, A.A.; Morris, S.M.; Tan, J.-C. Parts-per-billion (ppb) selective iodine sensors leveraging metal–organic framework nanoenvironment. *Mater. Today* **2022**. https://doi.org/10.1016/j.mattod.2022.07.001.
16. Rydosz, A.; Maciak, E.; Wincza, K.; Gruszczynski, S. Microwave-based sensors with phthalocyanine films for acetone, ethanol and methanol detection. *Sens. Actuators B Chem.* **2016**, *237*, 876–886.
17. Amoah, P.K.; Lin, P.; Baumgart, H.; Franklin, R.; Obeng, Y.S. Broadband dielectric spectroscopic detection of volatile organic compounds with ZnO nanorod gas sensors. *J. Phys. D Appl. Phys.* **2020**, *54*, 135104. https://doi.org/10.1088/1361-6463/abd3ce.
18. Amoah, P.K.; Hassan, Z.M.; Lin, P.; Redel, E.; Baumgart, H.; Obeng, Y.S. Broadband dielectric spectroscopic detection of ethanol: A side-by-side comparison of ZnO and HKUST-1 MOFs as sensing media. *Chemosensors* **2022**, *10*, 241.
19. Li, F.; Zheng, Y.; Hua, C.; Jian, J. Gas sensing by microwave transduction: Review of progress and challenges. *Front. Mater.* **2019**, *6*, 101. https://doi.org/10.3389/fmats.2019.00101.
20. *Broadband Dielectric Spectroscopy*; Woodward, W.H.H., Ed.; American Chemical Society: Washington, DC, USA, 2021; https://doi.org/10.1021/bk-2021-1375.
21. Badalyan, A.; Stahl, S.S. Cooperative electrocatalytic alcohol oxidation with electron-proton-transfer mediators. *Nature* **2016**, *535*, 406–410. https://doi.org/10.1038/nature18008.
22. Kremer, F.; Schönhals, A. *Broadband Dielectric Spectroscopy*, 1st ed.; Friedrich Kremer, A.S., Ed.; Springer: Berlin/Heidelberg, Germany, 2003; https://doi.org/10.1007/978-3-642-56120-7.

23. Entesari, K.; Ghiri, R.E.; Kaya, E. Broadband dielectric spectroscopy: Recent developments in microwave time-domain techniques. *IEEE Microw. Mag.* **2021**, *22*, 26–48. https://doi.org/10.1109/MMM.2021.3064100.

24. Collin, R.E. *Foundations for Microwave Engineering*, 2nd ed.; Wiley-Interscience, New York, NY, USA, 2001.

25. Wilson, P. *The Circuit Designer's Companion*; Newnes: Oxford, UK, 2012; https://doi.org/10.1016/c2010-0-66361-9.

26. Chen, X.; Zhang, K.; Hassan, Z.M.; Redel, E.; Baumgart, H. Charge transport, conductivity and seebeck coefficient in pristine and TCNQ loaded preferentially grown metal-organic framework films. *J. Phys. Condens. Matter* **2022**, *34*, abe72f.

27. Arslan, H.K.; Shekhah, O.; Wohlgemuth, J.; Franzreb, M.; Fischer, R.A.; Wöll, C. High-throughput fabrication of uniform and homogenous MOF coatings. *Adv. Funct. Mater.* **2011**, *21*, 4228–4231.

28. Calvo, J.J.; Angel, S.M.; So, M.C. Charge transport in metal–organic frameworks for electronics applications. *APL Mater.* **2020**, *8*, 050901. https://doi.org/10.1063/1.5143590.

29. Sundriyal, S.; Shrivastav, V.; Bhardwaj, S.K.; Mishra, S.; Deep, A. Tetracyanoquinodimethane doped copper-organic framework electrode with excellent electrochemical performance for energy storage applications. *Electrochim. Acta* **2021**, *380*, 138229.

30. Müller, K.; Fink, K.; Schöttner, L.; Koenig, M.; Heinke, L.; Wöll, C. Defects as color centers: The apparent color of metal–organic frameworks containing Cu2+-based paddle-wheel units. *ACS Appl. Mater. Interfaces* **2017**, *9*, 37463–37467. https://doi.org/10.1021/acsami.7b12045.

31. Wang, W.; Sharapa, D.I.; Chandresh, A.; Nefedov, A.; Heißler, S.; Heinke, L.; Studt, F.; Wang, Y.; Wöll, C. Interplay of electronic and steric effects to yield low-temperature CO oxidation at metal single sites in defect-engineered HKUST-1. *Angew. Chem. Int. Ed.* **2020**, *59*, 10514–10518.

32. Pozar, D.M. *Microwave Engineering*, 4th ed.; J. Wiley: Hoboken, NJ, USA, 2012.

33. Hassan, Z.M.A. The Photophysical Properties of Chromophores Assembled into Metal-Organic Framework Thin-Films. Ph.D. Thesis, Karlsruher Institut für Technologie (KIT), Karlsruhe, Germany, 2021.

34. Rivera-Torrente, M.; Filez, M.; Schneider, C.; van der Feltz, E.C.; Wolkersdörfer, K.; Taffa, D.H.; Wark, M.; Fischer, R.A.; Weckhuysen, B.M. Micro-spectroscopy of HKUST-1 metal–organic framework crystals loaded with tetracyanoquinodimethane: Effects of water on host–guest chemistry and electrical conductivity. *Phys. Chem. Chem. Phys.* **2019**, *21*, 25678–25689. https://doi.org/10.1039/C9CP05082E.

35. Strauss, I.; Mundstock, A.; Treger, M.; Lange, K.; Hwang, S.; Chmelik, C.; Rusch, P.; Bigall, N.C.; Pichler, T.; Shiozawa, H.; et al. Metal–organic framework Co-MOF-74-Based host–guest composites for resistive gas sensing. *ACS Appl. Mater. Interfaces* **2019**, *11*, 14175–14181. https://doi.org/10.1021/acsami.8b22002.

36. Talin, A.A.; Centrone, A.; Ford, A.C.; Foster, M.E.; Stavila, V.; Haney, P.; Kinney, R.A.; Szalai, V.; Gabaly, F.E.; Yoon, H.P.; et al. Tunable electrical conductivity in metal-organic framework thin-film devices. *Science* **2014**, *343*, 66–69. https://doi.org/10.1126/science.1246738.

37. Erickson, K.J.; Léonard, F.; Stavila, V.; Foster, M.E.; Spataru, C.D.; Jones, R.E.; Foley, B.M.; Hopkins, P.E.; Allendorf, M.D.; Talin, A.A. Thin film thermoelectric metal–organic framework with high seebeck coefficient and low thermal conductivity. *Adv. Mater.* **2015**, *27*, 3453–3459.

38. Liu, J.; Wächter, T.; Irmler, A.; Weidler, P.G.; Gliemann, H.; Pauly, F.; Mugnaini, V.; Zharnikov, M.; Wöll, C. Electric transport properties of surface-anchored metal-organic frameworks and the effect of ferrocene loading. *ACS Appl. Mater. Interfaces* **2015**, *7*, 9824–9830. https://doi.org/10.1021/acsami.5b01792.

39. Janczak, J.; Prochowicz, D.; Lewiński, J.; Fairen-Jimenez, D.; Bereta, T.; Lisowski, J. Trinuclear cage-like ZnII macrocyclic complexes: Enantiomeric recognition and gas adsorption properties. *Chem. A Eur. J.* **2016**, *22*, 598–609.

40. Deegan, M.M.; Dworzak, M.R.; Gosselin, A.J.; Korman, K.J.; Bloch, E.D. Gas storage in porous molecular materials. *Chem. A Eur. J.* **2021**, *27*, 4531–4547.

41. Collier-Oxandale, A.M.; Thorson, J.; Halliday, H.; Milford, J.; Hannigan, M. Understanding the ability of low-cost MOx sensors to quantify ambient VOCs. *Atmos. Meas. Tech.* **2019**, *12*, 1441–1460. https://doi.org/10.5194/amt-12-1441-2019.

42. Loera-Serna, S.; Oliver-Tolentino, M.A.; de Lourdes López-Núñez, M.; Santana-Cruz, A.; Guzmán-Vargas, A.; Cabrera-Sierra, R.; Beltrán, H.I.; Flores, J. Electrochemical behavior of [Cu3(BTC)2] metal–organic framework: The effect of the method of synthesis. *J. Alloy. Compd.* **2012**, *540*, 113–120.

43. Hendon, C.H.; Walsh, A. Chemical principles underpinning the performance of the metal–organic framework HKUST-1. *Chem. Sci.* **2015**, *6*, 3674–3683. https://doi.org/10.1039/C5SC01489A.

44. Chou, J. *Hazardous Gas Monitors: A Practical Guide to Selection, Operation and Applications*, 1st ed.; McGraw-Hill: New York, NY, USA, 2000.

45. Lamy, C.; Belgsir, E.M.; Léger, J.M. Electrocatalytic oxidation of aliphatic alcohols: Application to the direct alcohol fuel cell (DAFC). *J. Appl. Electrochem.* **2001**, *31*, 799–809. https://doi.org/10.1023/A:1017587310150.

46. Heinke, L.; Gu, Z.; Wöll, C. The surface barrier phenomenon at the loading of metal-organic frameworks. *Nature Communications* **2014**, *5*, 4562. https://doi.org/10.1038/ncomms5562.

47. Chevalier, V.; Martin, J.; Peralta, D.; Roussey, A.; Tardif, F. Performance of HKUST-1 Metal-Organic Framework for a VOCs mixture adsorption at realistic concentrations ranging from 0.5 to 2.5 ppmv under different humidity conditions. *J. Environ. Chem. Eng.* **2019**, *7*, 103131.

48. Gutmann, V.; Gutmann, V. *The Donor-Acceptor Approach to Molecular Interactions*; Springer: New York, NY, USA, 1978; Volume 228.

49. Tan, K.; Jensen, S.; Zuluaga, S.; Chapman, E.K.; Wang, H.; Rahman, R.; Cure, J.; Kim, T.-H.; Li, J.; Thonhauser, T.; et al. Role of hydrogen bonding on transport of coadsorbed gases in metal–organic frameworks materials. *J. Am. Chem. Soc.* **2018**, *140*, 856–859. https://doi.org/10.1021/jacs.7b09943.

50. Khakyzadeh, V.; Sediqi, S. The electro-oxidation of primary alcohols via a coral-shaped cobalt metal–organic framework modified graphite electrode in neutral media. *Sci. Rep.* **2022**, *12*, 8560. https://doi.org/10.1038/s41598-022-12200-w.

51. Guo, P.; Froese, C.; Fu, Q.; Chen, Y.-T.; Peng, B.; Kleist, W.; Fischer, R.A.; Muhler, M.; Wang, Y. CuPd mixed-metal HKUST-1 as a catalyst for aerobic alcohol oxidation. *J. Phys. Chem. C* **2018**, *122*, 21433–21440. https://doi.org/10.1021/acs.jpcc.8b05882.

52. Greco, R.; Tiburcio-Fortes, E.; Fernandez, A.; Marini, C.; Vidal-Moya, A.; Oliver-Meseguer, J.; Armentano, D.; Pardo, E.; Ferrando-Soria, J.; Leyva-Pérez, A. MOF-stabilized perfluorinated palladium cages catalyze the additive-free aerobic oxidation of aliphatic alcohols to acids. *Chem. A Eur. J.* **2022**, *28*, e202103781.

53. Bordiga, S.; Regli, L.; Bonino, F.; Groppo, E.; Lamberti, C.; Xiao, B.; Wheatley, P.S.; Morris, R.E.; Zecchina, A. Adsorption properties of HKUST-1 toward hydrogen and other small molecules monitored by IR. *Phys. Chem. Chem. Phys.* **2007**, *9*, 2676–2685. https://doi.org/10.1039/B703643D.

54. Rubio-Giménez, V.; Almora-Barrios, N.; Escorcia-Ariza, G.; Galbiati, M.; Sessolo, M.; Tatay, S.; Martí-Gastaldo, C. Origin of the chemiresistive response of ultrathin films of conductive metal–organic frameworks. *Angew. Chem. Int. Ed.* **2018**, *57*, 15086–15090.

55. Koo, W.-T.; Jang, J.-S.; Kim, I.-D. Metal-organic frameworks for chemiresistive sensors. *Chem* **2019**, *5*, 1938–1963. https://doi.org/10.1016/j.chempr.2019.04.013.

56. Ho, R.Y.N.; Liebman, J.F.; Valentine, J.S. Biological reactions of dioxygen: An introduction. In *Active Oxygen in Biochemistry*, Valentine, J.S., Foote, C.S., Greenberg, A., Liebman, J.F., Eds.; Springer: Dordrecht, The Netherlands, 1995; pp. 1–36. https://doi.org/10.1007/978-94-011-0609-2_1.

57. Cadman, L. Multi-Component Metal-Organic Frameworks. Ph.D. Thesis, University of Bath, Bath, UK, 2017.

58. Sun, L.; Hendon, C.H.; Minier, M.A.; Walsh, A.; Dincă, M. Million-fold electrical conductivity enhancement in Fe2(DEBDC) versus Mn2(DEBDC) (E = S, O). *J. Am. Chem. Soc.* **2015**, *137*, 6164–6167. https://doi.org/10.1021/jacs.5b02897.

59. Dhakshinamoorthy, A.; Asiri, A.M.; Garcia, H. Tuneable nature of metal organic frameworks as heterogeneous solid catalysts for alcohol oxidation. *Chem. Commun.* **2017**, *53*, 10851–10869. https://doi.org/10.1039/C7CC05927B.

60. Chaudhuri, P.; Hess, M.; Müller, J.; Hildenbrand, K.; Bill, E.; Weyhermüller, T.; Wieghardt, K. Aerobic oxidation of primary alcohols (including methanol) by Copper(II)− and Zinc(II)−Phenoxyl radical catalysts. *J. Am. Chem. Soc.* **1999**, *121*, 9599–9610. https://doi.org/10.1021/ja991481t.

61. Huang, Y.-R.; Liu, K.-H.; Mou, C.-Y.; Sun, C.-K. Relaxation dynamics of surface-adsorbed water molecules in nanoporous silica probed by terahertz spectroscopy. *Appl. Phys. Lett.* **2015**, *107*, 081607.

62. Sachdeva, S.; Koper, S.J.H.; Sabetghadam, A.; Soccol, D.; Gravesteijn, D.J.; Kapteijn, F.; Sudhölter, E.J.R.; Gascon, J.; de Smet, L.C.P.M. Gas phase sensing of alcohols by metal organic framework-polymer composite materials. *ACS Appl. Mater. Interfaces* **2017**, *9*, 24926–24935. https://doi.org/10.1021/acsami.7b02630.

63. Sutradhar, M.; Alegria, E.C.B.A.; Barman, T.R.; Guedes da Silva, M.F.C.; Liu, C.-M.; Pombeiro, A.J.L. 1D Copper(II)-Aroylhydrazone coordination polymers: Magnetic properties and microwave assisted oxidation of a secondary alcohol. *Front. Chem.* **2020**, *8*, 157. https://doi.org/10.3389/fchem.2020.00157.

64. Hazra, S.; Martins, L.M.D.R.S.; Guedes da Silva, M.F.C.; Pombeiro, A.J.L. Sulfonated Schiff base copper(ii) complexes as efficient and selective catalysts in alcohol oxidation: Syntheses and crystal structures. *RSC Adv.* **2015**, *5*, 90079–90088. https://doi.org/10.1039/C5RA19498A.

65. Polshettiwar, V.; Varma, R.S. Microwave-assisted organic synthesis and transformations using benign reaction media. *Acc. Chem. Res.* **2008**, *41*, 629–639. https://doi.org/10.1021/ar700238s.

66. Silva, T.F.S.; Martins, L.M.D.R.S. Recent advances in copper catalyzed alcohol oxidation in homogeneous medium. *Molecules* **2020**, *25*, 748.

67. Horikoshi, S.; Watanabe, T.; Narita, A.; Suzuki, Y.; Serpone, N. The electromagnetic wave energy effect(s) in microwave-assisted organic syntheses (MAOS). *Sci. Rep.* **2018**, *8*, 5151. https://doi.org/10.1038/s41598-018-23465-5.

68. Huang, K.; Liu, N.; Liu, C.; Yan, L. Preliminary analysis of chemical reaction under the radiation of electromagnetic wave. *Chin. Sci. Bull.* **2000**, *45*, 1821–1824. https://doi.org/10.1007/BF02886276.

69. Maes, B.; Marimuthu, T.; Alapour, S.; Friedrich, H.B. Microwave-assisted oxidation reaction of primary alcohols with sensitive functional groups to aldehydes using ruthenium diphosphorus complexes. *Arkivoc* **2020**, *2020*, 120–135. https://doi.org/10.24820/ark.5550190.p011.197.